Spin wave-assisted reduction in switching field of highly coercive iron-platinum magnets

Takeshi Seki[1], Kazutoshi Utsumiya[1], Yukio Nozaki[2], Hiroshi Imamura[3] & Koki Takanashi[1]

Recent rapid progress in spintronic and magnetic storage nanodevices has required nano-magnets to balance competing goals for high coercive field and low switching field. However, a decisive route for highly efficient magnetization switching has not been established yet. Here we propose a novel switching method using a spin wave of magnetic structures twisted in a nanometre scale. We have experimentally demonstrated extremely low field-magneti-zation switching in a highly coercive FePt by using a spin wave excited in a soft magnetic permalloy ($Ni_{81}Fe_{19}$), where permalloy is exchange-coupled to FePt through the interface. We can tune the switching field by varying the magnitude and frequency of the radio frequency magnetic field, and a significant decrease in switching field by one order of magnitude is achieved under the optimum conditions. The spin wave-assisted magnetization switching is a promising technique for ultralow-energy magnetization manipulation.

[1] Institute for Materials Research, Tohoku University, Sendai 980-8577, Japan. [2] Department of Physics, Keio University, Yokohama 223-8522, Japan. [3] National Institute of Advanced Industrial Science and Technology, Tsukuba 305-8568, Japan. Correspondence and requests for materials should be addressed to T.S. (email: go-sai@imr.tohoku.ac.jp).

A route simultaneously achieving competing goals for good thermal stability of magnetization (high coercive field H_c) and low switching field H_{sw} is indispensable for the further development of spintronic and magnetic storage nanodevices[1]. Energy-assisted switching[2–12], spin-transfer switching[13,14] and voltage-induced H_c modulation[15] are examined to overcome this predicament. One of the energy-assisted switching methods is microwave-assisted magnetization reversal (MAMR), which is considered to be a promising recording method for future ultrahigh density magnetic storage[2–9]. It applies a radio-frequency (rf) magnetic field H_{rf} to a highly coercive magnet to obtain induction of uniform magnetization precession to reduce H_{sw}. However, MAMR has an inherent undesirable characteristic. The frequency of H_{rf} is around the ferromagnetic resonance (FMR) frequency f_{FMR}, which is of the order of 100 GHz for a highly coercive magnet. This is a serious obstacle for practical applications. Indeed, although several papers[3–5] reported H_{sw} reduction at single-digit gigahertz frequencies using soft magnetic materials such as a Ni–Fe alloy with $f_{FMR} < 10$ GHz, a high excitation frequency > 10 GHz was required in the case of a highly coercive magnet with $f_{FMR} > 10$ GHz[7,8]. There are no reports of clear H_{sw} reduction for a highly coercive magnet at single-digit gigahertz frequencies. Thus, another way of reducing H_{sw} while maintaining high H_c is desired. The concept of magnetization switching presented here is based on the utilization of spin wave modes in a soft magnet to switch the magnetization in a hard magnet. A similar method has been theoretically proposed by Li et al.[16] and Fal et al.[17] However, there has been no experimental demonstration to date as far as we are aware. Here we show the significant reduction in H_{sw} of highly coercive FePt due to the spin wave excitation.

Results

Magnetic structure and FMR. We combined a hard magnetic FePt layer with a soft magnetic permalloy ($Fe_{19}Ni_{81}$; Py) layer, as schematically illustrated in Fig. 1a. In this FePt/Py bilayer, FePt has an uniaxial easy magnetization axis along the in-plane [001] direction. The magnetic moments in Py are spatially twisted after the magnetic field H has been applied in the opposite direction to the magnetic moments in FePt[18]. The Py layer thickness t_{Py} was varied in the range from 40 to 120 nm, whereas the FePt layer thickness was fixed at 10 nm. The full magnetization loop of an FePt/Py bilayer with $t_{Py} = 100$ nm (Fig. 1b) shows two steep decreases in magnetization. The first steep decrease at around $H = -100$ Oe corresponds to the twist of magnetic moments in Py. The second steep decrease at around $H = -1,600$ Oe means that the bilayer's magnetization has switched. The minor loop is superimposed on the full loop. After all the magnetizations has
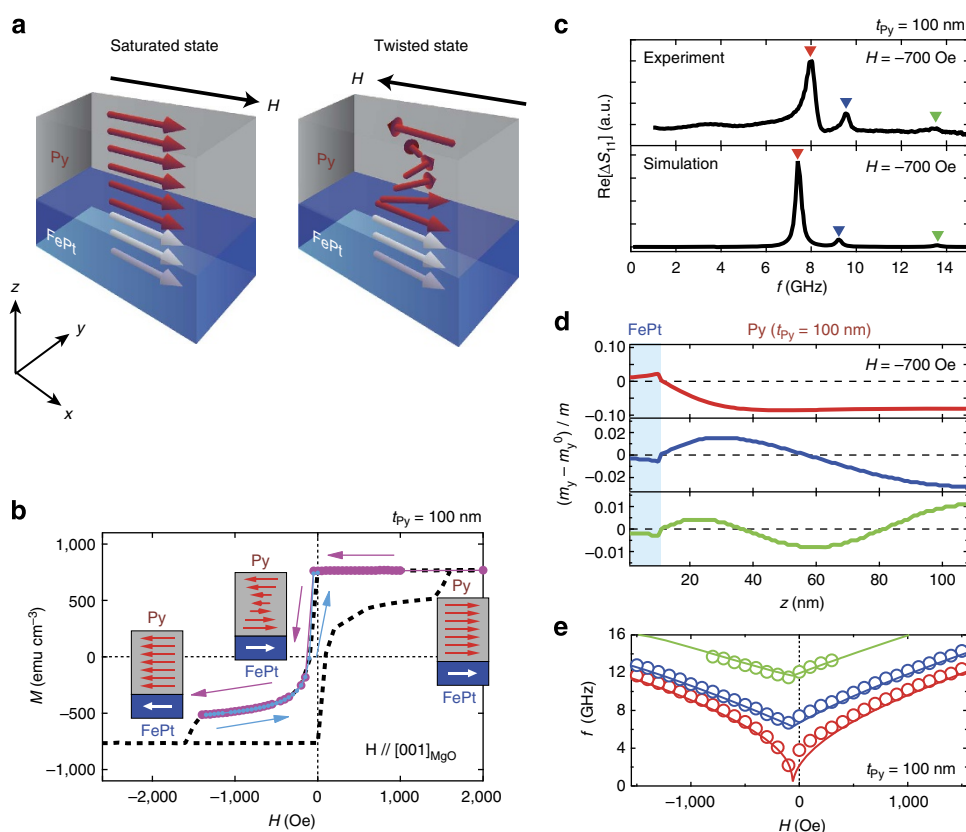

Figure 1 | Magnetization loops and FMR for an FePt/Py bilayer. (**a**) Illustrations of magnetic structures in an FePt/Py bilayer. The left (right) panel depicts the direction of magnetic moments in the saturated (twisted) state together with the coordinate axes. Magnetic field H was applied along the in-plane [001] direction of the MgO (110) substrate, which corresponds to the easy magnetization direction of FePt. (**b**) Magnetization full loop (dashed line) and minor loop for the bilayer with the Py layer thickness t_{Py} of 100 nm. For the minor loop measurements, $H = 50$ kOe was first applied to saturate all the magnetizations in the positive direction. Then, H was swept to $-1,400$ Oe (magenta circles) and back to zero (cyan circles). (**c**) FMR spectra of $t_{Py} = 100$ nm for experiment (upper panel) and simulation (lower panel) at $H = -700$ Oe. The triangles indicate the resonant frequencies. (**d**) Snapshots of the deviation of magnetic moments from the equilibrium position in the y direction $m_y - m_y^0$. The red, blue and green curves correspond to the first, second and third FMR peaks, respectively. These excitation modes are the PSSW modes with $n = 0$ (red), $n = 1$ (blue) and $n = 2$ (green), where n is the number of nodes. The interface between FePt and Py is located at $z = 10$ nm. (**e**) Experimentally obtained resonant frequencies of $n = 0$ (red), $n = 1$ (blue) and $n = 2$ (green) plotted as a function of H for $t_{Py} = 100$ nm (open circles). The simulated resonant frequencies are also shown by solid lines.

been saturated in the positive direction at $H = 50\,kOe$, H was swept to $-1,400\,Oe$ (magenta circles). Then, H was returned to zero (cyan circles). The minor loop is completely reversible without any hysteresis. This behaviour is well known as spring-back[19], indicating that FePt and Py are exchange-coupled through the interface and that the magnetic moments in Py are spatially twisted by applying H.

We measured the FMR spectra of the FePt/Py bilayers using a coplanar waveguide (CPW) and a vector network analyser[20,21] (see Methods). Figure 1c shows the FMR spectrum for $t_{Py} = 100\,nm$ at $H = -700\,Oe$ under the application of $H_{rf} = 6\,Oe$. We observed three resonant peaks at the frequencies $f = 8.0$, 9.5 and $13.5\,GHz$, as indicated by red, blue and green triangles, respectively. The shape of the experimental FMR spectrum is well reproduced by the simulation (for more details of experimental FMR spectra, see Supplementary Fig. S1). To classify the excited magnetization dynamics at each resonance, we plotted snapshots of the deviation of magnetic moments from the equilibrium position in Fig. 1d. The red, blue and green curves correspond to the first, second and third FMR peaks, respectively. These excitation modes are known as the perpendicular standing spin wave (PSSW) modes [22] with n nodes. Figure 1e shows the experimental results for the H dependence of resonant frequencies (open circles) together with the simulated results (solid lines). The simulated results were obtained using the calculation method reported by Livesey et al.[23] (for more details, see Methods). We successfully observed the higher-order PSSW modes, which have never been reported for previous experimental studies[24–26], and the frequencies of all modes agree well with the simulation. The present results are also in good agreement with

the simulation reported by Fal et al.[17] Looking at Fig. 1d carefully, one can see that the dynamics of magnetic moments in FePt are also induced by PSSW. In other words, depinning occurs in FePt due to the excitation of PSSW in Py. This leads us to the idea that high H_{rf} enhances the amplitude of PSSW and should reduce H_{sw} of the FePt/Py bilayer.

Spin wave-assisted magnetization switching. We micro-fabricated rectangular FePt/Py bilayer elements on the signal line of a CPW (Fig. 2a) to study the H_{sw} reduction by PSSW. The device resistance R depends on the direction of magnetic moments in the FePt/Py bilayer owing to the anisotropic mag-netoresistance effect[27,28]. Figure 2b shows the R–H curve for $t_{Py} = 100\,nm$ without H_{rf} being applied. When H was swept from positive to negative (denoted by red circles), R showed an abrupt decrease at $H = -175\,Oe$, reflecting the twist of magnetic moments in Py. R returned to the baseline resistance R_B at $H = H_{sw} = -2,050\,Oe$ (green arrows), where the magnetic moments of the bilayer were switched. Figure 2c displays ΔR–H curves for $t_{Py} = 100\,nm$ with $H_{rf} = 145\,Oe$, where ΔR is defined as $R - R_B$. No remarkable changes in H_{sw} were observed for $f = 6.0\,GHz$. However, the application of H_{rf} with $f = 8.0\,GHz$ reduced H_{sw} to $325\,Oe$. As f was increased from 8.0 to $12.5\,GHz$, H_{sw} monotonically increased. Small dips in ΔR appeared in the saturated state, which are indicated by orange triangles. A two-dimensional map of normalized ΔR as functions of H and f is shown in Fig. 2d. H was swept from positive to negative. The H_{sw} reduction was obtained in the wide range of f from 8 to $14\,GHz$. The small dip in ΔR has the same dispersion as that of PSSW in
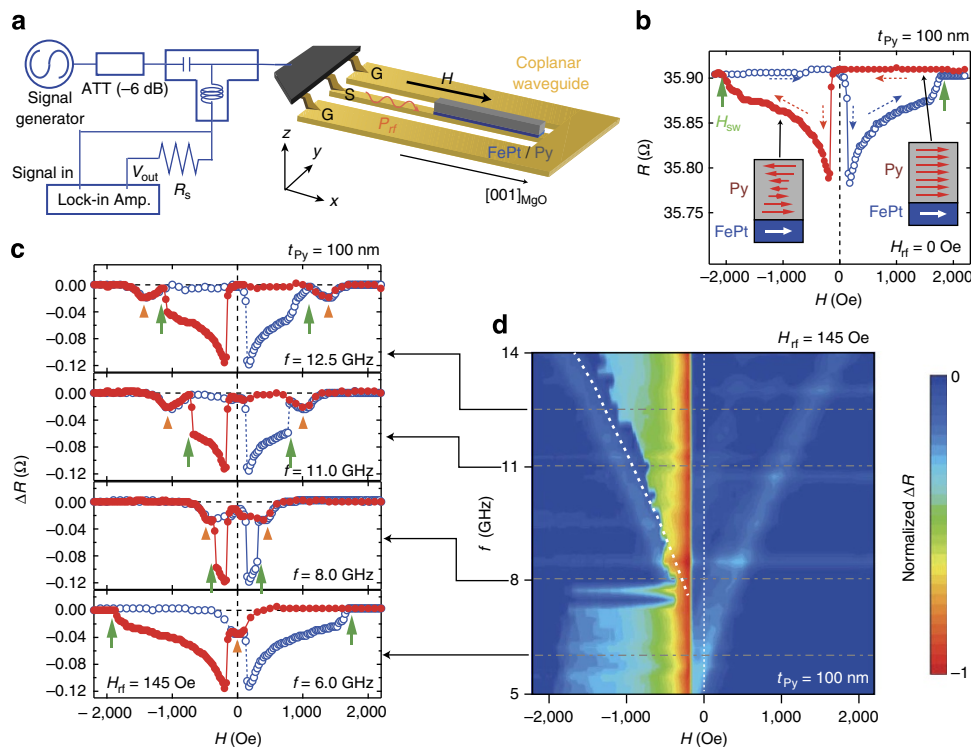
Figure 2 | Spin wave-assisted magnetization switching. (**a**) Schematic illustration of the device structure and measurement setup. The rf power was applied from a signal generator through the rf port of a bias-Tee. The device resistance R as a function of H was measured using a lock-in amplifier. R_s is a reference resistance of $1\,k\Omega$. The FePt/Py was designed to be rectangular, $2 \times 50\,\mu m^2$. (**b**) R–H curve for $t_{Py} = 100\,nm$ without the rf magnetic field H_{rf}. The green arrows denote the switching fields H_{sw}. (**c**) ΔR–H curves for $t_{Py} = 100\,nm$ under the application of $H_{rf} = 145\,Oe$, where ΔR is the resistance change from the baseline resistance. The frequencies f of H_{rf} were 12.5, 11.0, 8.0 and 6.0 GHz. The small dips in ΔR due to the excitation of PSSW are indicated by orange triangles. (**d**) Two-dimensional map of normalized ΔR as functions of H and f for $t_{Py} = 100\,nm$. H was swept from positive to negative. The white dotted line denotes the resonant frequency of PSSW with $n = 0$ in the twisted state of the microfabricated sample.

the saturated state. To understand what determined the value of H_{sw} at each f, we overlapped the resonant frequency of PSSW with $n = 0$ in the twisted state of the microfabricated sample (white dotted line). Note that the frequency dependence of H_{sw} qualitatively followed that of the resonant magnetic field of PSSW H_{PSSW}, indicating that magnetization switching was induced by PSSW as we expected.

Figure 3a shows the f dependence of H_{sw} for $t_{Py} = 100$ nm obtained experimentally (circles) and numerically (squares). The experimental results qualitatively coincide with the simulation. The largest reduction in H_{sw} was achieved at $f = 10$ GHz in the experiment, whereas the simulation showed the largest H_{sw} reduction at around $f = 9$ GHz. The simulated result has two local minima of H_{sw}. Analysing the PSSW mode contributing to the magnetization switching, we found that these two local minima originated from the PSSW modes with different n. Because the experiments were performed at room temperature, these two local minima of H_{sw} were smeared out. For both experiment and simulation, H_{rf} with low f is ineffective for H_{sw} reduction because the resonant magnetic field at such low f is so low that it cannot twist the magnetic moments enough to reduce H_{sw} at $H_{rf} = 91$ Oe. Spin wave-assisted magnetization switching was also attempted for the FePt/Py bilayer with $t_{Py} = 40$ nm. We did not observe any H_{sw} reduction even when $H_{rf} = 113$ Oe was applied (see Supplementary Fig. S2). This result provides two important facts: the excitation of the FMR mode in FePt does not contribute to the H_{sw} reduction (see Supplementary Fig. S3), and a thin Py layer is not effective for H_{sw} reduction.

Figure 3b shows H_{sw} as functions of f and H_{rf} for the FePt/Py bilayer with $t_{Py} = 120$ nm. The frequency giving the lowest H_{sw} decreased as H_{rf} was increased. We successfully achieved the largest reduction in H_{sw} from 2,000 to 250 Oe at $f = 7$ GHz and $H_{rf} = 134$ Oe (Fig. 3c). Let us introduce the rate of H_{sw} reduction defined as $\delta H_{sw} = H_{sw}/H_{sw}^0$, where H_{sw}^0 is H_{sw} without H_{rf}. According to the MAMR calculation reported by Zhu et al.[6], $H_{sw}^0 = 5.3\ H_{rf}$ and $H_{sw} = 1.5\ H_{rf}$. Consequently, δH_{sw} for MAMR

is about 0.27, which is twice as high as that of spin wave-assisted magnetization switching, $\delta H_{sw} = 0.13$.

Discussion

We examined the nonlinear magnetization dynamics in the FePt/Py bilayer because large H_{rf} was applied for spin wave-assisted switching. FMR spectra for the microfabricated device were also measured under the application of large H_{rf} (see Supplementary Fig. S4), and clear resonant peaks were observed as in the case of small H_{rf}. The linewidth of resonant peaks became broadened and the asymmetric peak shape was observed for large H_{rf}, which may be related to the nonlinear magnetization dynamics. However, more pronounced nonlinear effects, such as remarkable nonlinear frequency shift, were not observed. This is different from nonlinear magnetization dynamics observed in spin torque oscillators[29], where spatially uniform magnetization precession is induced by spin-polarized electric current. The precession frequency of a spin torque oscillator depends on the precession angle because the change in the precession angle leads to the large change in the effective field. On the other hand, the PSSW mode observed in this study is spatially non-uniform magnetization dynamics, and its precession frequency is mainly determined by the exchange field. The exchange field does not depend on the precession angle. Thus, the absence of the remarkable nonlinear frequency shift for the present devices is attributable to the less dependence of effective field on the precession angle.

An important point is that the PSSW modes were well defined even under the large H_{rf} application. To understand the magnetization dynamics during switching, the time evolution of magnetization switching behaviour was simulated numerically. Figure 4 shows the snapshots of simulated magnetic structures during magnetization switching under the application of $H_{rf} = 90$ Oe with $f = 10$ GHz (for more details, see Supplementary Movie 1 and Supplementary Table 1), where H was swept from 0 to $-1,500$ Oe, and the magnetization switching occurs in the H
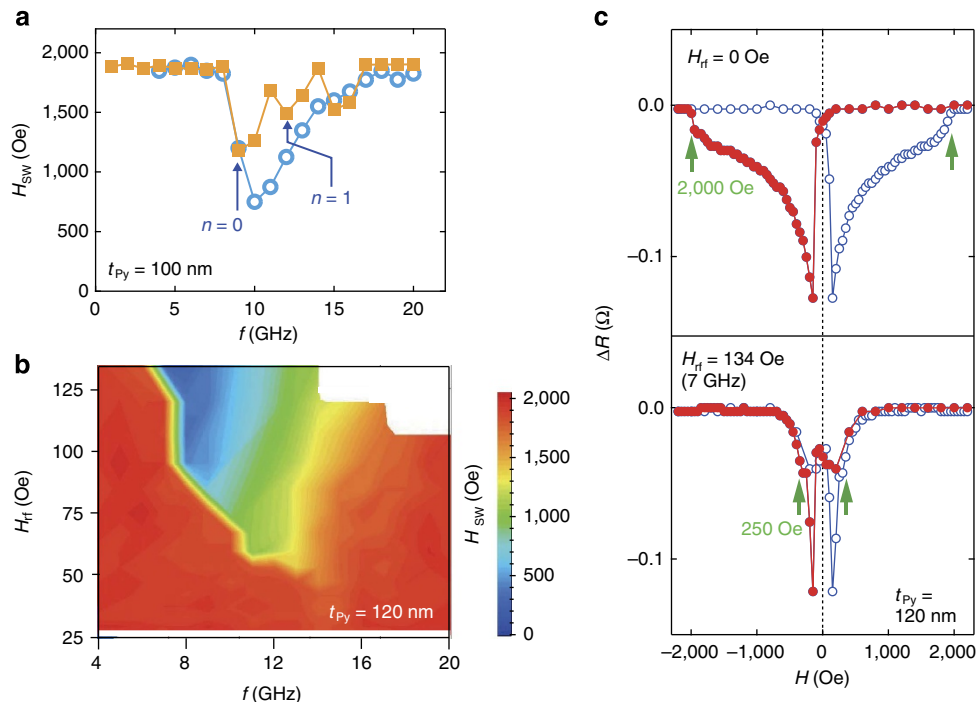
Figure 3 | Optimum conditions of H_{rf} and f for H_{sw} reduction. (a) H_{sw} as a function of f for $t_{Py} = 100$ nm (circles), where the value of H_{rf} was set to 91 Oe. Simulated H_{sw} as a function of f is also shown by closed squares. **(b)** Two-dimensional map of H_{sw} as functions of H_{rf} and f for $t_{Py} = 120$ nm. **(c)** ΔR–H curves for $t_{Py} = 120$ nm with $H_{rf} = 0$ Oe (top panel) and 134 Oe (bottom panel). The frequency of H_{rf} was 7 GHz.

range from $-1,250.5$ (Fig. 4a) to $-1,260$ Oe (Fig. 4f). The amplitude of the PSSW mode in Py is resonantly enhanced, which increases the precessional amplitude of FePt at the interface, and all the magnetic moments are finally switched. The PSSW mode with $n=0$ largely contributes to the H_{sw} reduction compared with the other modes ($n=1$ and 2). According to the simulated result (Fig. 3a), $n=1$ could also reduce H_{sw} at the resonant frequency, although the H_{sw} reduction is not so significant and is smeared out in the experiment. A reason for the large H_{sw} reduction by $n=0$ is the larger precession amplitude for $n=0$ than those for $n=1$ and 2 (see Fig. 1d and Supplementary Fig. S5). As shown in Fig. 4, the large amplitude magnetization precession in Py induces the large amplitude magnetization precession in FePt, which effectively switches the magnetization of FePt.

The numerical simulation indicates that the spin wave excitation leads to the magnetization switching in FePt. However, one might think that in the experiment, H_{sw} is not the real switching field of FePt, but the depinning field in FePt layer because depinning occurs in FePt under the large H_{rf} application. We confirmed that H_{sw} corresponded to the real switching field of FePt from the anisotropic magnetoresistance curves measured using different sequences of magnetic field sweep (see Supplementary Fig. S6). One might also suspect that the origin of H_{sw} reduction is the temperature rise due to the application of H_{rf}, that is, Joule heating by alternating current. However, this idea can be eliminated because R_B, which is a function of the device temperature, did not show any dependence on f (see Supplementary Fig. S7). The large H_{sw} reduction by spin wave excitation was also confirmed for the other devices (see Supplementary Table S2), indicating that the error in the rate of H_{sw} reduction is small. Because our results simultaneously achieved the competing goals of both high H_c and low H_{sw}, spin wave-assisted magnetization switching provides a new nanotechnology for information writing in a wide range of spintronic and magnetic storage applications.

Methods

Thin film preparation. Thin films were prepared on a MgO (110) single-crystal substrate. The stacking of the thin films was MgO (110) substrate/Fe (1 nm)/Au (40 nm)/FePt (10 nm)/Py (t_{Py})/Au (3 nm). The layers from Fe to FePt were deposited by using an ultrahigh vacuum (UHV) magnetron sputtering system (ULVAC, Inc.) equipped with high-purity targets of Fe (99.99%), Pt (99.99%) and Au (99.9%). The base pressure of the UHV magnetron sputtering system was below 2×10^{-7} Pa. A 1-nm thick Fe seed layer and a 40-nm thick Au buffer layer were deposited at ambient temperature. Subsequently, a 10-nm thick FePt layer was deposited on the Au buffer layer after the substrate temperature was set at 450 °C. Then, the film was transferred from the UHV magnetron sputtering chamber to an ion beam sputtering (IBS) system. In the IBS chamber, a Py layer followed by a 3-nm thick Au capping layer was deposited on the FePt layer at ambient temperature. The compositions of FePt and Py were determined to be $Fe_{48}Pt_{52}$ and $Ni_{81}Fe_{19}$, respectively, by electron probe X-ray microanalysis. The epitaxial growth of Au, FePt and Py layers with the (110) preferential crystallographic orientation was confirmed by X-ray diffraction. The X-ray diffraction patterns also indicated the formation of the $L1_0$ ordered structure in the FePt layer. The magnetization loops of the thin films were measured at 295 K using a superconducting quantum interference device magnetometer.

FMR measurement. The FMR measurement was carried out at room temperature using a CPW and a vector network analyser. A thin film with a FePt/Py bilayer was put onto the CPW consisting of Cr/Au layers, and the CPW was connected to the rf circuit employing a two-terminal rf probe. The rf power P_{rf} of 0 dBm was applied to the signal line, which induced a transverse rf magnetic field of $H_{rf} \sim 6$ Oe, and the change in the reflected signal was detected with the vector network analyser. The value of S_{11} is defined as the ratio of the reflected voltage to the input voltage. The frequency dependence of S_{11} was measured under the application of H, which was applied along the in-plane easy magnetization direction.

Device fabrication and electrical measurement. Rectangular-shaped FePt/Py elements were prepared by using a conventional microfabrication process. First, a negative-type electron beam (EB) resist was spin-coated onto the thin film and patterned into the shape of the CPW by EB lithography (ELS-7500; Elionix Inc.). The width and length of the signal line of CPW were 4 and 50 μm, respectively. After exposure of the EB resist followed by development, the thin film was milled by argon ions through the resist mask. The EB resist was then spin-coated onto the CPW-shaped film and patterned into a rectangular shape with the size of 2×50 μm², which was located on top of the signal line of the CPW-shaped film. The CPW-shaped film was again milled by argon ions. The ion milling was stopped at the top of the Au buffer layer, which was monitored by secondary ion mass spectroscopy. Finally, the Au buffer layer remained as the signal and ground lines of the CPW, and the rectangular FePt/Py element was prepared on the signal line. This rectangular shape induces the shape anisotropy of Py. Because the long axis of rectangle is the same as the in-plane [001] direction of the FePt layer, both uniaxial easy magnetization axes of FePt and Py are in the same direction. The microfabricated device was connected to the rf-compatible circuit via a two-terminal rf probe, and P_{rf} was applied from a signal generator through the rf port of a bias-Tee after -6 dB attenuation. The application of P_{rf} induced H_{rf} in the y–z plane of the FePt/Py element. The device resistance was simultaneously measured using a lock-in amplifier.

Numerical simulation. Numerical simulation was carried out by solving the Landau–Lifshitz–Gilbert (LLG) equation by using the conventional fourth-order
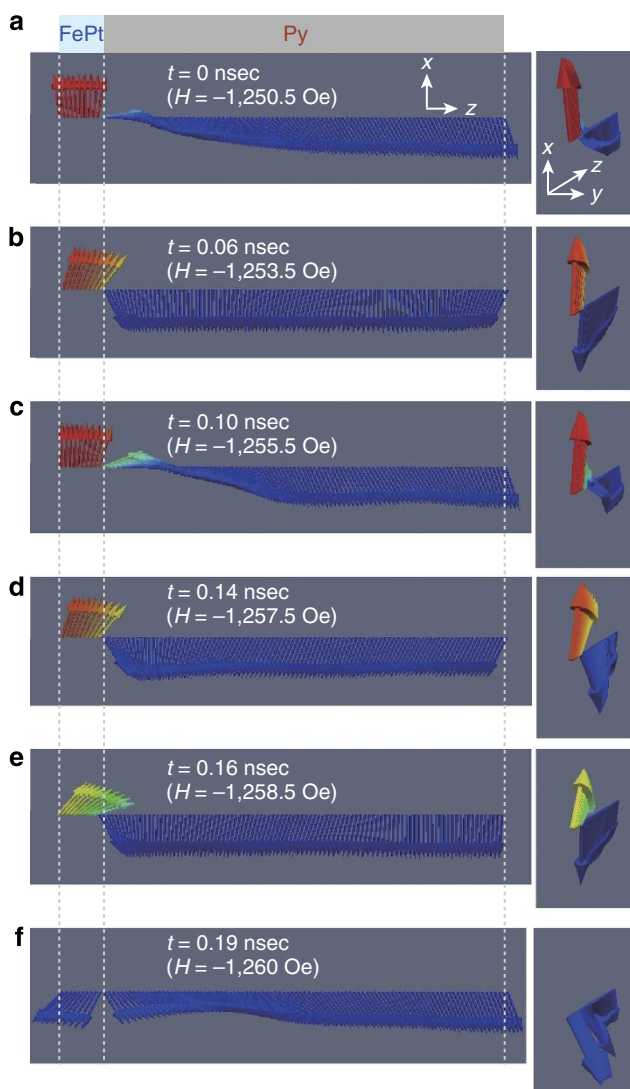
Figure 4 | Time evolution of magnetization switching behaviour. Simulated magnetic structures in the x–z plane (left panels) and the x–y plane (right panels), where $H_{rf} = 90$ Oe with $f = 10$ GHz was applied. H was swept from 0 to $-1,500$ Oe, and the magnetization switching occurs in the range from $H = -1,250.5$ Oe (**a**) to $H = -1,260$ Oe (**f**). (**a–f**) The time-evolved snapshots of magnetic structures during the magnetization switching.

Runge–Kutta algorithm. The effective magnetic field in the LLG equation is the vector sum of the anisotropy field, magnetostatic field, exchange field, H, and H_{rf}. In the present numerical study, we considered an exchange-coupled FePt/Py bilayer of infinite size in the film plane. The thicknesses of FePt and Py were fixed at 10 and 98 nm, respectively. The film was discretized into 1-nm thick infinite plates, and each plate was assumed to have a uniform magnetization vector. The saturation magnetizations of FePt and Py were determined to be 1000 and 800 emu cm^{-3}, respectively, from the magnetization measurement. The inter- and intra-layer exchange constants of FePt/Py, A_{int}, A_{FePt} and A_{Py}, were chosen to be 1.0×10^{-7}, 1.0×10^{-6} and 1.3×10^{-6} erg cm^{-1}, respectively, so as to reproduce the experimental magnetization loop. The small value of A_{int} results from the slight oxidation and/or the contamination on the FePt surface during the sample transfer from the UHV magnetron sputtering system to the IBS system with breaking the vacuum. The uniaxial anisotropy constant of FePt K_{FePt} was assumed to be 3.3×10^6 erg cm^{-3}, which was determined from the magnetic field required to switch FePt in the lithographically patterned device (see Fig. 2b), whereas K_{Py} was set to 1.0×10^3 erg cm^{-3}. One may consider that $K_{FePt} = 3.3 \times 10^6$ erg cm^{-3} is small. The one-dimensional model often leads to the underestimation of K_{FePt} to reproduce H_{sw} because in experiment H_{sw} is generally much smaller than the anisotropy field. The experimental value of K_{FePt} was about 2.5×10^7 erg cm^{-3}. The Gilbert damping constants for Py and FePt were 0.008 and 0.02, respectively. To evaluate the H_{sw} reduction under the H_{rf} application, we set H_{rf} to 90 Oe. When H_{sw} as a function of f was evaluated, the magnetization was initially magnetized along $+x$ direction. The magnetization was relaxed for 10 ns under H_{rf} applied along the y axis. The magnetization curve under the H_{rf} application was then calculated sweeping the dc magnetic field along the x direction. The field sweep velocity was 50 Oe ns^{-1}. H_{sw} was defined as the magnetic field at which the magnetization of the FePt layer became zero. To obtain the f dependence of H_{sw}, f was varied in the range from 1 to 20 GHz.

Using the same parameters as those for the magnetization switching simulation, we calculated the stable magnetic structure at each H by solving the LLG equation. For these stable magnetic structures, we solved the eigenvalue equations corresponding to the linear response to the small H_{rf} and obtained the resonant frequencies. To construct the eigenvalue equations, we employed the local rotated frame where the coordinates are rotated about the z axis such that the new x axis points in the same direction as the local magnetization vectors.

References

1. Chappert, C., Fert, A. & Nguyen Van Dau, F. The emergency of spin electronics in data storage. *Nat. Mater.* **6,** 813–823 (2007).
2. Thirion, C., Wernsdorfer, W. & Mailly, D. Switching of magnetization by nonlinear resonance studied in single nanoparticles. *Nat. Mater.* **2,** 524–527 (2003).
3. Woltersdorf, G. & Back, C. H. Microwave assisted switching of single domain Ni$_{80}$Fe$_{20}$ elements. *Phys. Rev. Lett.* **99,** 227207 (2007).
4. Nembach, H. T. *et al.* Microwave assisted switching in a Ni$_{81}$Fe$_{19}$ ellipsoid. *Appl. Phys. Lett.* **90,** 062503 (2007).
5. Moriyama, T. *et al.* Microwave-assisted magnetization switching of Ni80Fe20 in magnetic tunnel junctions. *Appl. Phys. Lett.* **90,** 152503 (2007).
6. Zhu, J. -G., Zhu, X. & Tang, Y. Microwave assisted magnetic recording. *IEEE Trans. Magn.* **44,** 125–131 (2008).
7. Nozaki, Y., Narita, N., Tanaka, T. & Matsuyama, K. Microwave-assisted magnetization reversal in a Co/Pd multilayer with perpendicular magnetic anisotropy. *Appl. Phys. Lett.* **95,** 082505 (2009).
8. Yoshioka, T. *et al.* Microwave-assisted magnetization reversal in a perpendicularly magnetized film. *Appl. Phys. Exp.* **3,** 013002 (2010).
9. Boone, C. T., Katine, J. A., Marinero, E. E., Pisana, S. & Terris, B. D. Microwave-assisted magnetic reversal in perpendicular media. *IEEE Magn. Lett.* **3,** 3500104 (2012).
10. Atkinson, D. & Cowburn, R. P. Heat-assisted magnetization switching in elongated submicrometer Permalloy structures. *Appl. Phys. Lett.* **85,** 1386–1388 (2009).
11. Rottmayer, R. E. *et al.* Heat-assisted magnetic recording. *IEEE Trans. Magn.* **42,** 2417–2421 (2006).
12. Prejbeanu, I. L. *et al.* Thermally assisted MRAM. *J. Phys.: Condens. Matter* **19,** 165218 (2007).
13. Tsoi, M. *et al.* Excitation of a magnetic multilayer by an electric current. *Phys. Rev. Lett.* **80,** 4281–4284 (1998).
14. Myers, E. B., Ralph, D. C., Katine, J. A., Louie, R. N. & Buhrman, R. A. Current-induced switching of domains in magnetic multilayer devices. *Science* **285,** 867–870 (1999).
15. Weisheit, M. *et al.* Electric field-induced modification of magnetism in thin-film ferromagnets. *Science* **315,** 349–351 (2007).
16. Li, S. *et al.* Microwave assisted magnetization reversal in composite media. *Appl. Phys. Lett.* **94,** 202509 (2009).
17. Fal, T. J., Livesey, K. L. & Camley, R. E. Domain wall and microwave assisted switching in an exchange spring bilayer. *J. Appl. Phys.* **109,** 093911 (2011).
18. Utsumiya, K., Seki, T. & Takanashi, K. Magnetic properties of L1$_0$-FePt/permalloy exchange-spring films. *J. Appl. Phys.* **110,** 103911 (2011).
19. Kneller, E. F. & Hawig, R. The exchange-spring magnet: a new material principle for permanent magnets. *IEEE Trans. Magn.* **27,** 3588–3600 (1991).
20. Counil, G. *et al.* Spin wave contributions to the high-frequency magnetic response of thin films obtained with inductive methods. *J. Appl. Phys.* **95,** 5646–5652 (2004).
21. Novosad, V. *et al.* Magnetic vortex resonance in patterned ferromagnetic dots. *Phys. Rev. B* **72,** 024455 (2005).
22. Demokritov, S. O., Hillebrands, B. & Slavin, A. N. Brillouin light scattering studies of confined spin waves: linear and nonlinear confinement. *Phys. Reports* **348,** 441–489 (2001).
23. Livesey, K. L., Crew, D. C. & Stamps, R. L. Spin wave valve in an exchange spring bilayer. *Phys. Rev. B* **73,** 184432 (2006).
24. Fullerton, E. E., Jiang, J. S., Grimsditch, M., Sowers, C. H. & Bader, S. D. Exchange-spring behavior in epitaxial hard/soft magnetic bilayers. *Phys. Rev. B* **58,** 12193–12200 (1998).
25. Grimsditch, M. *et al.* Exchange-spring systems: coupling of hard and soft ferromagnets as measured by magnetization and Brillouin light scattering. *J. Appl. Phys.* **85,** 5901–5904 (1999).
26. Schmool, D. S., Apolinário, A., Casoli, F. & Albertini, F. Ferromagnetic resonance study of Fe/FePt coupled films with perpendicular anisotropy. *IEEE Trans. Magn.* **44,** 3087–3090 (2008).
27. Takanashi, K., Kamiguchi, Y., Fujimori, H. & Motokawa, M. Magnetization and magnetoresistance of Fe/ Gd ferrimagnetic multilayer films. *J. Phys. Soc. Jpn.* **61,** 3721–3731 (1992).
28. Mibu, K., Nagahama, T., Shinjo, T. & Ono, T. Magnetoresistance of Bloch-wall-type magnetic structures induced in NiFe/CoSm exchange-spring bilayers. *Phys. Rev. B* **58,** 6442–6446 (1998).
29. Kiselev, S. I. *et al.* Microwave oscillations of a nanomagnet driven by a spin-polarized current. *Nature* **425,** 380–383 (2003).

Acknowledgements

Author contributions

T.S. and K.T. planned and supervised the study. T.S. and K.U. carried out the sample preparation and the measurement of magnetic and transport properties. Y.N. and H.I. contributed to the theoretical modelling for the interpretation and performed the micromagnetic simulation. All of the authors contributed to the physical understanding, data analysis and manuscript preparation.

Additional information